Theoretical and Mathematical Physics, **144**(2): 1117–1127 (2005)

EVOLUTION OF OPTICAL PULSES IN FIBER LINES WITH LUMPED NONLINEAR DEVICES AS A MAPPING PROBLEM

S. Boscolo,* S. A. Derevyanko,* S. K. Turitsyn,* A. S. Kovalev,† and M. M. Bogdan†

We analyze the steady-state propagation of optical pulses in fiber transmission systems with lumped nonlinear optical devices (NODs) placed periodically in the line. For the first time to our knowledge, a theoretical model is developed to describe the transmission regime with a quasilinear pulse evolution along the transmission line and the point action of NODs. We formulate the mapping problem for pulse propagation in a unit cell of the line and show that in the particular application to nonlinear optical loop mirrors, the steady-state pulse characteristics predicted by the theory accurately reproduce the results of direct numerical simulations.

Keywords: dispersive systems with point nonlinearity, mapping problem, autosolitons

1. Introduction

Solitons in an optical fiber arise from a balance between the spreading effect of the fiber group-velocity dispersion and the nonlinear focusing effect of the fiber intensity-dependent refractive index. Conventional solitons [1] (i.e., propagating in fibers with a uniform dispersion) and dispersion-managed (DM) solitons [2], [3] (i.e., propagating in fibers with a periodic variation of the dispersion) have been a topic of intensive investigation in the last few decades because of their potential application as information carriers in optical communications. But upgrading existing terrestrial fiber links to operate at high data transmission rates generally requires using short pulses and consequently strong dispersion management (the definition of the dispersion map strength parameter S can be found, e.g., in [3]), whose strength values are well outside the range where stable propagation of DM solitons has been observed [4]. In the regime of high dispersion map strengths, which is usually called the quasilinear regime, carrier pulses experience periodically large temporal broadening, their intensity hence changes rapidly along the fiber, and the accumulated effect of the instantaneous fiber nonlinearity consequently tends to be averaged out. In some sense, this scheme is opposite to soliton or DM soliton transmission, where fiber nonlinearity plays an important role in preserving the pulse shapes during propagation.

It is known that degradation of the optical signals in a fiber communication system can be mitigated by using one or more regenerators within the system. Recently, the periodic in-line deployment of nonlinear optical devices (NODs), such as nonlinear loop mirrors (NOLMs), semiconductor saturable absorbers, and semiconductor amplifier-based devices, has been demonstrated to be an effective technique for all-optical signal regeneration [5]–[7], which may achieve stable pulse propagation and virtually unlimited transmission distances in high-speed, strongly DM systems [6]. It was shown numerically in [5], [6] that under certain conditions, the interplay between fiber dispersion, the lumped nonlinearity provided by in-line NOLMs, and the action of linear control elements, such as optical filters, leads to the formation of autosolitons, which are

*Photonics Research Group, School of Engineering and Applied Science, Aston University, Birmingham B4 7ET, United Kingdom, e-mail: boscolsa@aston.ac.uk, s.derevyanko@aston.ac.uk, s.k.turitsyn@aston.ac.uk.

†Verkin Institute for Low Temperature Physics and Engineering, 61103 Kharkov, Ukraine, e-mail: kovalev@ilt.kharkov.ua, bogdan@ilt.kharkov.ua.

Translated from Teoreticheskaya i Matematicheskaya Fizika, Vol. 144, No. 2, pp. 277–289, August, 2005.

periodically reproduced at the output of each segment of the transmission line. The term "autosolitons" here means robust localized pulses with the parameters prescribed by the system properties, which occur in models combining conservative and dissipative, dispersive and nonlinear terms [8].

In this paper, for the first time to our knowledge, a theory is developed to describe signal transmission in DM fiber transmission systems in the quasilinear regime with point NODs placed periodically in the line. We formulate the mapping problem for carrier pulse propagation in a unit cell of the transmission line. Without loss of generality, as specific realizations of the NODs, we consider power-law devices (PLDs) and NOLMs. In the case of PLDs, we derive an analytic solution of the mapping problem for the fixed points in some special limits. In the case of NOLMs, we apply a variational approach to determine the steady-state pulse characteristics and show that the theory accurately reproduces the features observed in full numerical simulations.

2. Basic model

We consider the optical pulse evolution in a cascaded transmission system with periodic variations of dispersion and nonlinearity, frequency filtering, and NOD management. In this case, pulse propagation can be described by the perturbed nonlinear Schrödinger equation

$$i\frac{\partial E}{\partial z} - \frac{1}{2}\beta_2(z)\frac{\partial^2 E}{\partial t^2} + \sigma(z)|E|^2 E = iG(z,|E|^2)E, \tag{1}$$

where $E(z,t)$ is the slowly varying pulse envelope in the comoving system of coordinates, $\beta_2(z)$ represents the variation in the group-velocity dispersion due to dispersion compensation and is assumed to be a periodic function of z with the period L, $\beta_2(z) = \beta_2(z+L)$, and σ is the fiber nonlinearity coefficient. It is customary to express β_2 in terms of the associated dispersion coefficient D via $\beta_2 = -\lambda^2 D/(2\pi c_0)$, where λ is the carrier wavelength, c_0 is the speed of light, and D is measured in ps/(nm·km). The function $G(z,|E|^2)$ accounts for the signal attenuation due to fiber loss, the signal amplification by optical amplifiers, the action of filters, and the nonlinear gain at the NODs; it can be represented as

$$\begin{aligned} G(z,|E|^2) = & -\gamma(z) + \sum_k \delta(z-kZ_{\rm a})\biggl\{\exp\biggl[\int_{(k-1)Z_{\rm a}}^{kZ_{\rm a}} dz\,\gamma(z)\biggr] - 1\biggr\} + \\ & + \sum_k \delta(z-kZ_{\rm f})[h(t) * -1] + \sum_k \delta(z-kZ_0)[f(|E|^2) - 1]. \end{aligned} \tag{2}$$

In Eq. (2), we assume that amplifiers, filters, and NODs are placed periodically in the system with the respective periods $Z_{\rm a}$, $Z_{\rm f}$, and Z_0. The delta-function terms are compact representations of the jump conditions at the amplifier, filter, and NOD locations, with the understanding that the delta functions sample any function $q(E)$ on the left, namely,

$$\int_{kZ_\beta^-}^{kZ_\beta^+} dz\,\delta(z-kZ_\beta)q(E) = q(E(kZ_\beta^-,t)),$$

where we introduce the notation $Z_\beta^\pm = Z_\beta \pm \epsilon$ in the limit $\epsilon \to 0$. The coefficient $\gamma = 0.05\log(10)\alpha$ is the fiber loss coefficient that accounts for the signal attenuation along the fiber span before the kth amplifier, α is given in dB/km, and

$$\exp\biggl[\int_{(k-1)Z_{\rm a}}^{kZ_{\rm a}} dz\,\gamma(z)\biggr] - 1$$

is the amplification coefficient after the fiber span between the $(k-1)$th and kth amplifiers. The function $h(t) = \mathcal{F}^{-1}[\hat{h}(\omega)]$ is the inverse Fourier transform of the filter transfer function, and $*$ represents the Fourier convolution. The NODs are specified by their power-dependent transfer function $f(P)$. Hereafter, we focus on PLDs and loss(gain)-unbalanced fiber NOLMs. The transfer function for such devices can be written in the form

$$f(P) = \begin{cases} aP^s & \text{for PLD,} \\ a\sin(bP)e^{icP} & \text{for NOLM,} \end{cases} \tag{3}$$

where $s \in \mathbb{R}$ and $a, b, c \in \mathbb{R}^+$ are some given constants.

3. Linear propagation regime and the mapping problem

To simplify the full model given by system (1), we make some justified physical assumptions. In this section, we analyze the case of linear propagation in a fiber, when we can neglect the nonlinear term in (1). Such a propagation regime corresponds to the case where the nonlinear length $L_{\mathrm{NL}} = (\sigma P_0)^{-1}$ (P_0 is the signal peak power) in the fiber is much larger than the local dispersion length $L_{\mathrm{D}} = T^2/|\beta_2|$ (T is the pulse width). Next, we can eliminate the linear loss and gain term by introducing a periodic pointwise discontinuous function $Q(z)$, defined as

$$Q(z) = \begin{cases} \exp\bigl[-\int_{(k-1)Z_{\mathrm{a}}}^{z} dz'\,\gamma(z')\bigr], & (k-1)Z_{\mathrm{a}} < z < kZ_{\mathrm{a}}, \\ 1, & z = kZ_{\mathrm{a}}^{+}. \end{cases} \tag{4}$$

Substituting $E(z,t) = Q(z)U(z,t)$ then brings (1) to

$$i\frac{\partial U}{\partial z} - \frac{1}{2}\beta_2(z)\frac{\partial^2 U}{\partial t^2} = i\biggl\{\sum_k \delta(z - kZ_{\mathrm{f}})[h(t) * -1] + \sum_k \delta(z - kZ_0)[f(\alpha_k^2|U|^2) - 1]\biggr\}U, \tag{5}$$

where $\alpha_k = Q[kZ_0 \bmod Z_{\mathrm{a}}]$ is a structural factor accounting for possible relative displacements of the amplifiers with respect to the NODs. In what follows, we assume that each NOD is placed immediately after an amplifier and therefore $\alpha_k = 1$.

The transformation of a pulse after propagation in one segment of the transmission line can be considered the mapping of the input pulse into the output pulse. If we consider an element of the transmission line that includes a NOD given by (3), a piece of linear fiber of length Z_0, and m filters, the signal map, defined up to a phase factor μ, can be represented as

$$e^{i\mu}U_{n+1}(t) = \int_{-\infty}^{+\infty} dt'\,K(t-t';Z_0)f(|U_n(t')|^2)U_n(t'), \quad n = 0, 1, \ldots . \tag{6}$$

Here, the signal is taken at the NOD input point nZ_0^- after any device preceding the NOD, and the kernel K is

$$K(t-t';Z_0) = \frac{1}{2\pi}\int_{-\infty}^{+\infty} dt''\,H(t-t'-t'')F(t'';Z_0), \tag{7}$$

where $H(t)$ represents the action of the filters,

$$H(t) = \mathcal{F}^{-1}[\hat{h}^m(\omega)], \tag{8}$$

and $F(t;Z_0)$ is the linear propagator of the uniform equation corresponding to Eq. (1),

$$F(t;Z_0)=\sqrt{\frac{i}{B_0}}e^{-it^2/(2B_0)},\qquad B_0=\int_{nZ_0}^{(n+1)Z_0}dz\,\beta_2(z). \tag{9}$$

In (9), B_0 is the total accumulated dispersion. We note that $H(t)\to\sqrt{2\pi}\delta(t)$ as $m\to 0$ (no filtering) and $F(t;Z_0)\to\sqrt{2\pi}\delta(t)$ as $B_0\to 0$ (full dispersion compensation). For simplicity in what follows, we consider Gaussian filters specified by

$$\hat{h}(\omega)=e^{-\omega^2/(2\Omega_{\rm f}^2)}, \tag{10}$$

where $\Omega_{\rm f}$ is the filter bandwidth. It is easy to verify that in such a case, K in (7) takes the form

$$K(t-t';Z_0)=\sqrt{G}\sqrt{\frac{i}{2\pi(B_0+im/\Omega_{\rm f}^2)}}\exp\left[-\frac{i(t-t')^2}{2(B_0+im/\Omega_{\rm f}^2)}\right], \tag{11}$$

where we insert an excess gain G to account for compensation of the signal energy losses introduced by the NODs and filters in the system.

From the transmission standpoint, it is desirable to find a steady-state propagation regime (if it exists) in which an optical pulse propagating along the transmission line is reproduced periodically at the output of each element of the line. This corresponds to determining a fixed point of map (6). Therefore, to find the steady-state pulse shape $U(t)$, we must solve a nonlinear integral equation, which stems from (6) if we set $U_{n+1}(t)=U_n(t)=U(t)$. When the steady-state pulse is stable, any initial signal gradually evolves toward it after some maps.

4. Power-law devices

In this section, we analyze the mapping problem defined in (6) when the NOD is a PLD specified by (3). Using some trial function to describe the signal $U(t)$, we can reduce the mapping integral equation in (6) to a set of algebraic equations for the signal parameter maps. Here, we use a Gaussian ansatz for the pulse shape, choosing a trial function in the form

$$U(t)=A\exp\left(-\frac{t^2}{2T^2}+iCt^2+i\xi\right), \tag{12}$$

where $A=\sqrt{P_0}$, T, C, and ξ describe the respective peak amplitude, width, chirp parameter, and phase shift of the pulse ($A,T\in\mathbb{R}^+$, $C,\xi\in\mathbb{R}_0$). Map (6) preserves the form of the pulse, and substituting ansatz (12) in (6) yields

$$\begin{aligned}
A_{n+1}&=\frac{a\sqrt{G}A_n^{2s+1}}{D_n^{1/4}},\\
T_{n+1}^2&=\frac{D_n}{(2s+1)/T_n^2+(m/\Omega_{\rm f}^2)[4C_n^2+(2s+1)^2/T_n^4]},\\
C_{n+1}&=\frac{(1-2B_0C_n)C_n-B_0(2s+1)^2/(2T_n^4)}{D_n},
\end{aligned} \tag{13}$$

where

$$D_n=(1-2B_0C_n)^2+\frac{B_0^2(2s+1)^2}{T_n^4}+\frac{m}{\Omega_{\rm f}^2}\left[\frac{4mC_n^2}{\Omega_{\rm f}^2}+\frac{2(2s+1)}{T_n^2}+\frac{m(2s+1)^2}{\Omega_{\rm f}^2T_n^4}\right],$$

$n = 0, 1, \ldots$. We note that phase factor μ in (6) is here chosen to compensate the phase shift $(\xi_{n+1} - \xi_n)$ arising from propagation along the line element. It can be seen from Eq. (13) that when $m/\Omega_f^2 \to 0$ and $B_0 \to 0$, any value of the chirp parameter is admitted, while the pulse amplitude is raised to the power $2s + 1$ and the pulse width is scaled by $1/\sqrt{2s+1}$, as could be expected. We can find the fixed points of map (13) analytically in some special limit cases. An interesting limit is the case where no filters are included in the transmission line or the filter bandwidth is very large, and then $m/\Omega_f^2 \to 0$. In this case, for fixed a, s, $B_0 \neq 0$, and G, map (13) has just one fixed point,

$$A = \left(\frac{2s+1}{a^4 G^2}\right)^{1/(8s)}, \qquad T = (2s+1)^{1/4}\sqrt{\left|\frac{B_0(s+1)}{s}\right|},$$
$$C = -\frac{s}{2B_0(s+1)}, \qquad s > -\frac{1}{2}, \quad s \neq 0. \tag{14}$$

Applying a linear stability analysis [9], we find that fixed point (14) is unstable for every s. We note that the eigenvalues of the linearized system associated with (13) depend on s only through (14).

Another interesting limit of system (13) is the case where the fiber dispersion is fully compensated along the line, and then $B_0 \to 0$. In this case, for fixed a, s, $m/\Omega_f^2 \neq 0$, and G, map (13) admits three fixed point solutions,

$$A = \left(\frac{|2s+1|}{a^2 G}\right)^{1/(4s)}, \qquad T = \sqrt{\frac{m(2s+1)}{2\Omega_f^2 s}}, \qquad C = 0, \qquad s < -\frac{1}{2} \quad \text{or} \quad s > 0, \tag{15}$$

$$A = (a^2 G)^{1/4}, \qquad T \geq \sqrt{\frac{m}{2\Omega_f^2}}, \qquad C = \pm\sqrt{\frac{1}{2T^2}\left(\frac{\Omega_f^2}{m} - \frac{1}{2T^2}\right)}, \qquad s = -1. \tag{16}$$

For fixed point (15), the eigenvalues of the linearized system associated with (13) are

$$\lambda_1 = 2s + 1, \qquad \lambda_2 = \frac{1}{2s+1}, \qquad \lambda_3 = \frac{1}{(2s+1)^2}. \tag{17}$$

It is straightforward to verify that fixed point (15) is stable for $s = -1$. The eigenvalues of the linearized system corresponding to fixed points (16) depend on T and m/Ω_f^2, and the stability of (16) can therefore be studied in terms of these two parameters.

5. Nonlinear optical loop mirrors

In this section, we consider the case where the NOD is a NOLM specified by (3) (see [10] for the description and operational principle of the NOLM). First, we analyze the mapping problem defined in (6) for continuous-wave (CW) signals. Then, we show the feasibility of stable autosoliton propagation in strongly DM systems guided by in-line NOLMs, directly simulating basic propagation model (1) numerically. Finally, applying a variational principle to Eq. (6), we describe the steady-state pulse characteristics observed in the numerical simulations.

5.1. Continuous-wave analysis. Taking the signal in the form

$$U(t) \equiv U_0 = \sqrt{P_0}e^{i\phi} \tag{18}$$

with the constants P_0 and ϕ, we obtain the power map

$$P_{0,n+1} = a^2 G \sin^2(bP_{0,n})P_{0,n} \tag{19}$$

from Eq. (6). It is understood that the CW approximation in (18) might hold only in the limit when the signal spectral bandwidth is much smaller than the effective spectral bandwidth for the system $\Omega_{\text{eff}} = \sqrt{m/[\Omega_{\text{f}}^2(B_0^2 + m^2/\Omega_{\text{f}}^4)]}$. For a stable steady state to exist, the conditions

$$P_{0,n+1} = P_{0,n}, \qquad \left|\frac{\partial P_{0,n+1}}{\partial P_{0,n}}\right|_{P_{0,n+1}=P_{0,n}} \le 1 \tag{20}$$

must be satisfied. Criteria (20) yield the relations

$$(a^2 G)^{-1} = \sin^2(bP_{0,n}), \qquad -1 \le \cot(bP_{0,n})bP_{0,n} \le 0, \tag{21}$$

which can then be evaluated numerically to yield the range of $bP_{0,n}$ that is stable. The illustrated CW stability analysis was proposed in [10]. But because it is based only on power considerations, this approach is not accurate.

We now generalize the CW analysis to include phase considerations. The problem can be handled as follows. We take the signal in the form

$$U(t) = U_0 + \delta U(t), \quad |\delta U| \ll |U_0|, \tag{22}$$

with U_0 given by (18). We then substitute (22) in Eq. (6) and expand transfer function (3) about U_0 to obtain

$$e^{i\mu}U_{0,n+1} = a\sqrt{G}\sin(bP_{0,n})e^{icP_{0,n}}U_{0,n}, \tag{23}$$

$$\begin{aligned} e^{i\mu}\delta U_{n+1}(t) = a\sin(bP_{0,n})e^{icP_{0,n}}\int_{-\infty}^{+\infty} dt'\, K(t-t';Z_0)\times \\ \times\left\{[1+(b\cot(bP_{0,n})+ic)P_{0,n}]\delta U_n(t') + \right. \\ \left. +(b\cot(bP_{0,n})+ic)P_{0,n}e^{2i\phi_n}\delta U_n^*(t')\right\}. \end{aligned} \tag{24}$$

If we now set

$$a\sqrt{G}\sin(bP_{0,n}) = 1, \qquad \mu = cP_{0,n}, \tag{25}$$

then it follows from (23) that $U_{0,n+1} = U_{0,n} = U_0$ is a fixed point of the map. We note that the first condition in (25) corresponds to the first relation in (21). Equation (24) and its complex conjugate can be used to study the stability of U_0. After straightforward calculations, we obtain the continuous spectrum of the system eigenvalues in the form

$$\begin{aligned} \lambda_{1,2}(\omega) = e^{-m\omega^2/(2\Omega_{\text{f}}^2)}\left\{(1+\cot(bP_0)bP_0)\cos\left(\frac{B_0\omega^2}{2}\right) - cP_0\sin\left(\frac{B_0\omega^2}{2}\right)\pm\right. \\ \pm\left[\left((c^2P_0^2-(1+\cot(bP_0)bP_0)^2)\sin\left(\frac{B_0\omega^2}{2}\right)-\right.\right. \\ \left.\left.-2cP_0(1+\cot(bP_0)bP_0)\cos\left(\frac{B_0\omega^2}{2}\right)\right)\sin\left(\frac{B_0\omega^2}{2}\right)+(\cot(bP_0)bP_0)^2\right]^{1/2}\Bigg\}, \end{aligned} \tag{26}$$

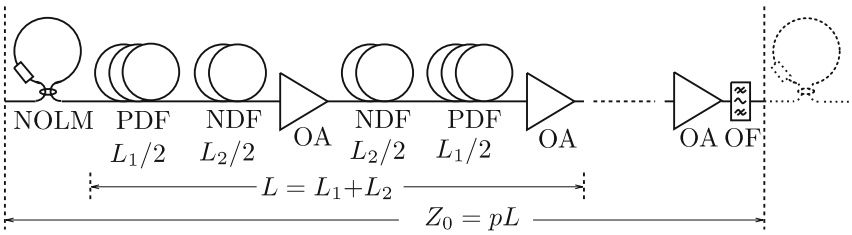

Fig. 1. One element of the periodic transmission system.

$\omega \in [-\infty, +\infty]$, where 1 and 2 index the two branches of the spectrum. We note that $\lambda_{1,2}(\omega)$ depend on the NOLM parameters via the ratio c/b, where $c/b \in (1, +\infty)$. For fixed B_0, $m/\Omega_{\rm f}^2$, c/b, and bP_0, the stability of the fixed point U_0 is ensured provided the condition $|\lambda_{1,2}(\omega)| \le 1\ \forall\omega$, $i = 1, 2$, is satisfied. In the limit $B_0 \to 0$, it is easy to verify that U_0 is stable for the values of bP_0 that satisfy the second relation in (21) and for any $m/\Omega_{\rm f}^2$ and c/b. In the general case where $B_0 \ne 0$, $|\lambda_{1,2}(\omega)|$ can be evaluated numerically to obtain the range of parameters where U_0 is stable. But we point out that the CW analysis, which does not account for the pulse shape, cannot be used to infer the stability of finite-width pulses propagating in the system. This should be done numerically.

5.2. Full numerical simulations. The sample transmission scheme used to integrate Eq. (1) numerically is depicted in Fig. 1. The transmission line is composed of an equal number of positive (anomalous) dispersion fiber (PDF) segments and negative (normal) dispersion fiber (NDF) segments. The dispersion map consists of an alternation of a PDF–NDF block and a mirror NDF–PDF block. Fiber parameters of practical importance ($D_1 = 15\,\text{ps/(nm·km)}$, $\sigma_1 = 1.84\,(\text{W·km})^{-1}$, $\alpha_1 = 0.22\,\text{dB/km}$, $D_2 = -71.2\,\text{ps/(nm·km)}$, $\sigma_2 = 4.28\,(\text{W·km})^{-1}$, and $\alpha_2 = 0.65\,\text{dB/km}$) are used for the PDF and the NDF [6]. We note that the fiber nonlinearity is included in the calculations.

An optical amplifier (OA), which compensates the fiber loss, follows each of the two blocks. The high values of the local dispersion of the fibers, together with the short pulse widths that are typically used to operate the system at high data rates, result in high map strengths ($S \gg 1$), which are beyond the range where DM solitons exist [4].

An NOLM is placed in the transmission line after every integer number p of dispersion map periods, $Z_0 = pL$. We note that $B_0 = \langle\beta_2\rangle Z_0 = -\lambda^2\langle D\rangle Z_0/(2\pi c_0)$ in this case ($\langle\,\cdot\,\rangle$ denotes the average over the dispersion compensating period L). In the sample configuration considered here, $Z_0 = 391\,\text{km}$ and $p = 5$. A single ($m = 1$) Gaussian optical filter (OF) is placed after the amplifier before the NOLM location.

The loss-unbalanced NOLM configuration is used as an example, and preamplification of the input pulses to the NOLM is used (see [6] for details). The parameters a, b, and c in transfer function (3) have the respective values 0.06373, $1.823\,\text{W}^{-1}$, and $1.839\,\text{W}^{-1}$. The NOLM acts as a saturable absorber [10] and hence filters out low-intensity radiation from the higher-power pulses. This allows restoring the pulse amplitude and shape [5], [6]. Following [6], the system is operated such that the peak power of the steady-state pulses (if any exist) is in the region slightly past the first peak of the CW power characteristic of the NOLM. In this region, the NOLM provides negative feedback control of the pulse amplitude [10], which may enable stabilization of the pulse amplitude fluctuations [6]. Of course, such a consideration does not guarantee stable pulse propagation in the system and is used here only to reduce the system parameter space where we seek the steady-state pulses.

Figure 2 shows an example of pulse evolution in the system, measured stroboscopically at the NOLM input point. In this example, an unchirped Gaussian pulse with the peak power $P_0 = 1.15\,\text{W}$ (corresponding to 3.5 mW at the starting point of the transmission) and the full-width-at-half-minimum (FWHM) pulse width $T_{\rm FWHM} = 5\,\text{ps}$ is launched into the system. The system parameters are $\langle D\rangle = 0.009\,\text{ps/(nm·km)}$,

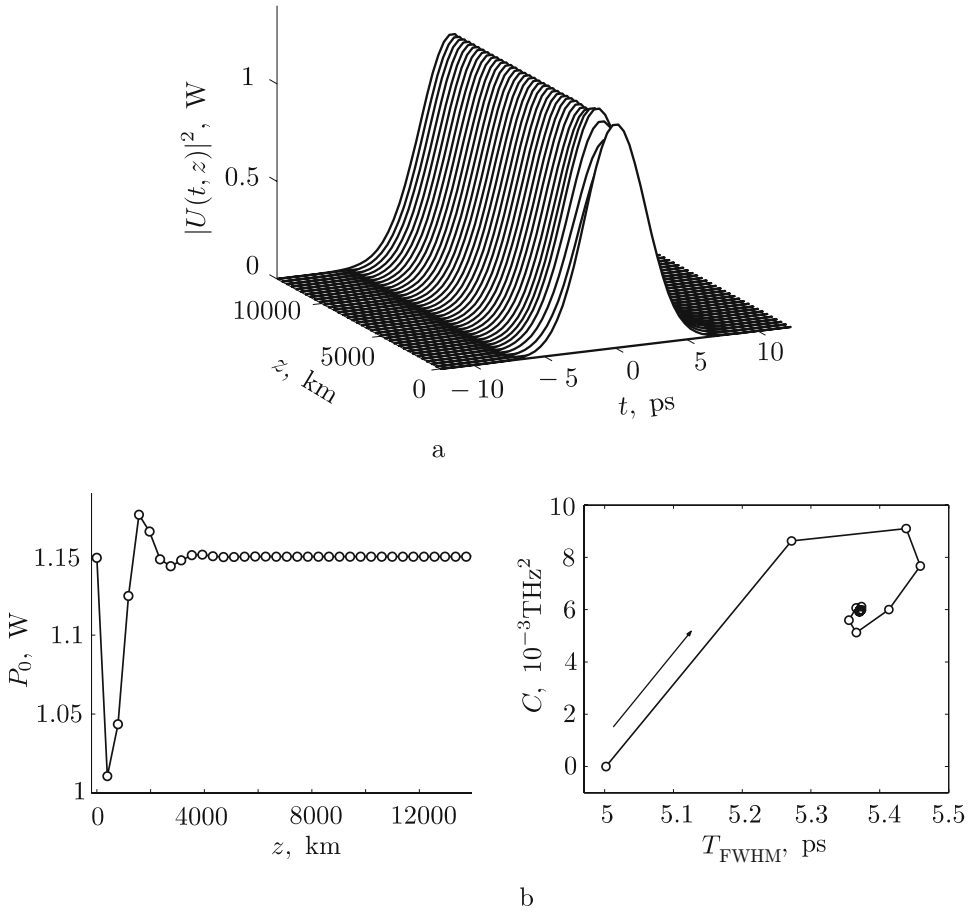

Fig. 2. Stroboscopic pulse evolution as viewed at the NOLM input: (a) Evolution of the intensity profile and (b) evolution of the pulse peak power (left) and acquisition of the steady state in the plane FWHM pulse width–chirp parameter (right).

$\delta\nu_{\text{f}} = \sqrt{\log 2}\Omega_{\text{f}}/\pi = 0.1\,\text{THz}$, and $G = 627.0$ (28.0 dB). The pulse chirp parameter is calculated as

$$C = \frac{\operatorname{Im}\int_{-\infty}^{+\infty} dt\, U^2 (U_t^*)^2}{\int_{-\infty}^{+\infty} dt\, |U|^4}.$$

It can be seen from Fig. 2 that the pulse settles to a steady state after a short initial transition distance. This result demonstrates the feasibility of stable pulse propagation in the system and indicates that using in-line NOLMs converts the quasilinear transmission regime into an autosoliton transmission regime, which is strictly nonlinear [6]. We note that the same stroboscopic picture as that in Fig. 2 can be obtained by simply iterating map (6).

We also determined the tolerable limits of the stable pulse propagation in terms of the filter bandwidth and the path-averaged dispersion of the line. The results are shown in Fig. 3, where $\delta\nu_{\text{f}}$ and $\langle D\rangle$ are varied within a practical range of values. In Fig. 3, G is chosen such that the steady-state pulse peak power is approximately 1.15 W at the NOLM input.

5.3. Variational approach and comparison with the full numerical simulations. As pointed out in Sec. 3, to find a steady-state pulse propagation regime, we must solve map (6) for the fixed points. But when NOLMs are used, solving the mapping problem analytically is a difficult task because of the specific

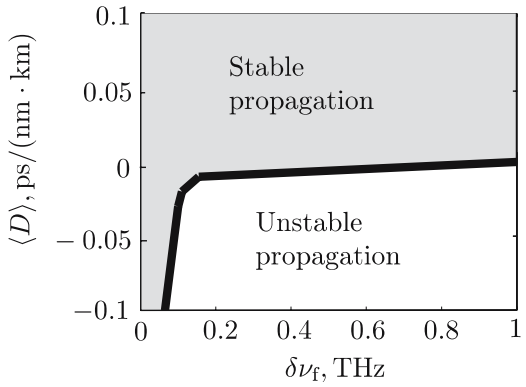

Fig. 3. Limits of stable pulse propagation in the filter bandwidth–average dispersion plane.

nonlinear transfer function of the NOLM. Therefore, we here apply a simplified variational approach. We notice from the full numerical simulation that the steady-state pulse shape at the NOLM input point can always be fitted well by a Gaussian profile. We therefore choose a trial input pulse $U(t)$ for the map as a Gaussian-shaped pulse with the (yet unknown) peak power P_0, root-mean-square (RMS) width T_{RMS}, and RMS chirp parameter C_{RMS},

$$U_n(t) = \sqrt{P_0}\exp\left(-\frac{t^2}{4T_{\mathrm{RMS}}^2} + iC_{\mathrm{RMS}}t^2\right). \tag{27}$$

The output of the map $U_{n+1}(t)$ given by Eq. (6) is generally non-Gaussian but has a close shape and depends on the parameters of the input signal, $U_{n+1} = U_{n+1}(t; P_0, T_{\mathrm{RMS}}, C_{\mathrm{RMS}})$. We now require that the peak power, pulse width, and chirp of the output signal coincide with those of the input Gaussian signal. This provides a system of transcendental equations for the sought parameters P_0, T_{RMS}, and C_{RMS},

$$\begin{aligned}
P_0 &= \frac{1}{\sqrt{2\pi}T_{\mathrm{RMS}}}\int_{-\infty}^{+\infty} dt\,|U_{n+1}(t; P_0, T_{\mathrm{RMS}}, C_{\mathrm{RMS}})|^2,\\
T_{\mathrm{RMS}}^2 &= \frac{\int_{-\infty}^{+\infty} dt\,t^2|U_{n+1}(t; P_0, T_{\mathrm{RMS}}, C_{\mathrm{RMS}})|^2}{\int_{-\infty}^{+\infty} dt\,|U_{n+1}(t; P_0, T_{\mathrm{RMS}}, C_{\mathrm{RMS}})|^2},\\
C_{\mathrm{RMS}} &= \frac{\mathrm{Im}\int_{-\infty}^{+\infty} dt\,U_{n+1}^2(t; P_0, T_{\mathrm{RMS}}, C_{\mathrm{RMS}})(\partial_t U_{n+1}^*(t; P_0, T_{\mathrm{RMS}}, C_{\mathrm{RMS}}))^2}{\int_{-\infty}^{+\infty} dt\,|U_{n+1}(t; P_0, T_{\mathrm{RMS}}, C_{\mathrm{RMS}})|^4}.
\end{aligned} \tag{28}$$

If the solution of system (28) exists, then it provides a variational approximation for the parameters of the steady-state pulse. In particular, we can use the Gaussian ansatz with the found values of P_0, T_{RMS}, and C_{RMS} as an approximation of the steady-state pulse shape.

The predictions of the variational model (Eqs. (27) and (28)) and the iterative numerical integration of map (6) have been compared with the results of the full numerical simulations. The steady-state pulse peak power, RMS width, and RMS chirp parameter are plotted in Fig. 4 as functions of the filter bandwidth for $\langle D\rangle = 0.009\,\mathrm{ps/(nm{\cdot}km)}$ and the same values of G as in Fig. 3. The results agree well, especially for the pulse width and the chirp parameter. The discrepancies in the pulse amplitude between the solutions of Eq. (6) and the full numerical simulations occurring for small values of $\delta\nu_{\mathrm{f}}$ (of the order of 6% at maximum) can be attributed to the effect of the nonlinearity in the transmission fibers, which is neglected in model (6), being more important for small filter bandwidths. For larger $\delta\nu_{\mathrm{f}}$, the deviation of model (6) from the full numerical simulations does not exceed 0.6%, which fully justifies the linear assumption underlying Eq. (6) in

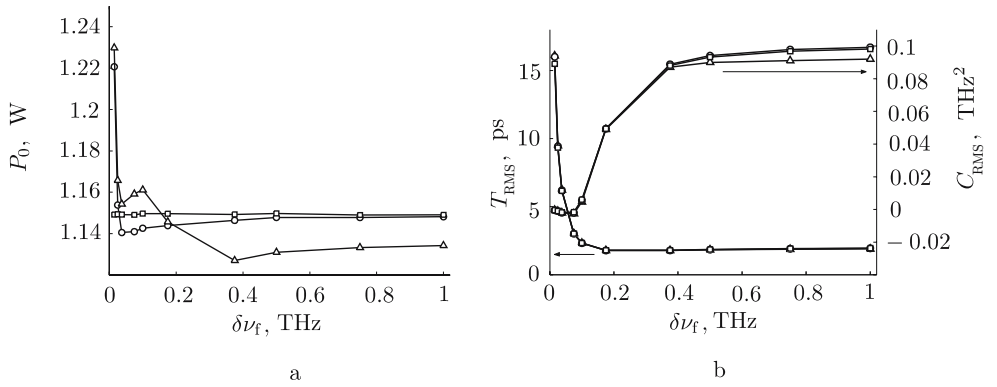

Fig. 4. Characteristics of the steady state: (a) pulse peak power and (b) RMS pulse width (left axis) and RMS chirp parameter (right axis) at the NOLM input versus filter bandwidth (circles, mapping equation; triangles, variational model; squares, full numerical simulations).

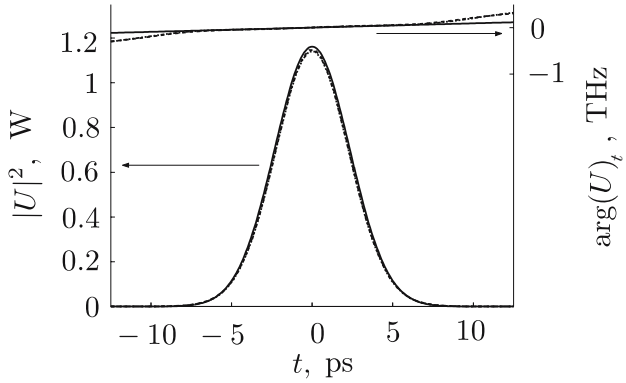

Fig. 5. Intensity (left axis) and chirp (right axis) of the steady-state pulse at the NOLM input (dotted line, mapping equation; solid line, variational model; dashed line, full numerical simulations).

this filter bandwidth range. The deviation of the variational model from either the full numerical simulations or model (6) does not exceed 2% in the bandwidth range where the linear assumption is entirely justified.

The steady-state intensity profile and chirp (first time derivative of the phase) of the input pulse to the NOLM are plotted in Fig. 5 for $\delta\nu_{\rm f} = 0.1\,$THz. The results from the variational model agree well with the full numerical results and the results from Eq. (6) in the central part of the pulse.

6. Conclusion

We have developed a theoretical model to describe the steady-state pulse propagation in DM fiber transmission systems in the quasilinear regime with periodic in-line deployment of NODs. In the particular application to NOLMs, we have demonstrated numerically that autosoliton formation can be observed in such systems as a result of a balance between the effects of dispersion in the transmission fibers, linear control by optical filters, and nonlinear focusing in the NOLMs. We have used a variational principle to determine the steady-state pulse characteristics and have shown that the theoretical analysis accurately reproduces the results of the full numerical simulations.

Acknowledgments. This work was supported in part by the NATO Collaborative Linkage Program (Grant No. PST.CLG.980068).

REFERENCES

1. A. Hasegawa and Y. Kodama, *Opt. Lett.*, **15**, 1443–1445 (1990).
2. I. Gabitov and S. K. Turitsyn, *Opt. Lett.*, **21**, 327–329 (1996).
3. N. J. Smith, F. M. Knox, N. J. Doran, K. J. Blow, and I. Bennion, *Electron. Lett.*, **32**, 54–55 (1996).
4. J. H. B. Nijhof, N. J. Doran, W. Forysiak, and A. Berntson, *Electron. Lett.*, **34**, 481–482 (1998).
5. S. Boscolo, J. H. B. Nijhof, and S. K. Turitsyn, *Opt. Lett.*, **25**, 1240–1242 (2000).
6. S. Boscolo, S. K. Turitsyn, and K. J. Blow, *IEEE Photon. Technol. Lett.*, **14**, 30–32 (2002).
7. D. Rouvillain, P. Brindel, E. Seguineau, L. Pierre, O. Leclerc, H. Choumane, G. Aubin, and J. L. Oudar, *Electron. Lett.*, **38**, 1113–1114 (2002).
8. B. S. Kerner and V. V. Osipov, *Autosolitons* [in Russian], Nauka, Moscow (1991); English transl.: *Autosolitons*: *A New Approach to Problems of Self-Organization and Turbulence*, Kluwer, Dordrecht (1994).
9. J. D. Logan, *Applied Mathematics*: *A Contemporary Approach*, Wiley, New York (1987).
10. N. J. Smith and N. J. Doran, *J. Opt. Soc. Am. B*, **12**, 1117–1125 (1995).